Title
Control of Magnetic Bearings for Rotor Unbalance With Plug-In Time-Varying Resonators

Journal
Journal of Dynamic Systems Measurement and Control, 138(1)

ISSN
0022-0434

Authors
Kang, Christopher
Tsao, Tsu-Chin

Publication Date
2016

DOI
10.1115/1.4031575

Peer reviewed

Christopher Kang
Mechatronics and Controls Laboratory,
Department of Mechanical and
Aerospace Engineering,
University of California, Los Angeles,
Los Angeles, CA 90095
e-mail: chriskang@g.ucla.edu

Tsu-Chin Tsao
Professor
Mechatronics and Controls Laboratory,
Department of Mechanical and
Aerospace Engineering,
University of California, Los Angeles,
Los Angeles, CA 90095
e-mail: ttsao@seas.ucla.edu

Control of Magnetic Bearings for Rotor Unbalance With Plug-In Time-Varying Resonators

Rotor unbalance, common phenomenon of rotational systems, manifests itself as a periodic disturbance synchronized with the rotor's angular velocity. In active magnetic bearing (AMB) systems, feedback control is required to stabilize the open-loop unstable electromagnetic levitation. Further, feedback action can be added to suppress the repeatable runout but maintain closed-loop stability. In this paper, a plug-in time-varying resonator is designed by inverting cascaded notch filters. This formulation allows flexibility in designing the internal model for appropriate disturbance rejection. The plug-in structure ensures that stability can be maintained for varying rotor speeds. Experimental results of an AMB–rotor system are presented. [DOI: 10.1115/1.4031575]

1 Introduction

A well-known problem affecting spinning rotors is that of rotor unbalance [1]. Mass imperfections in the shaft results in a periodic disturbance force synchronous to the rotor's angular velocity. In traditional rotor systems, the rotor is supported by journal bearings which are fit snugly over the outer diameter of the rotor. The unbalance force causes mechanical wear in the bearings as well as the force to be transmitted into the rotor housing.

AMBs are a commonly used replacement due to their mechanical benefits. AMBs are electromagnets arranged in a ring configuration levitating the rotor at the center of the stator. This magnetic levitation allows the bearing to be contact-less, which eliminates the issue of mechanical wear, friction, and thus eliminates the need for lubricants [2]. AMBs are, however, open-loop unstable requiring the need for robust feedback controls [1]. Furthermore, because AMBs do not rigidly support the rotor, they are susceptible to runout or radial vibrations excited by rotor unbalance. Still, they have successfully been implemented in such systems as power generation [3], flywheels [4], mills [5], and even on the impeller of an artificial heart [6].

In AMB–rotor systems, one important control design criterion is the stability of the system. Closed-loop stability exists as a criterion due to safety concerns during high rotor speed operations. These strategies must also be effective as the rotor speed changes over the entire operating range. Many approaches exist in this regard including feedforward compensation where the system matrices for a number of rotation speeds were determined offline to generate the proper compensation signal scheduled by rotor speed [7]. In Ref. [8], H_∞ controllers were designed for segments of the operational speed range. These approaches could prove cumbersome to implement for large rotor speed ranges. Linear quadratic Gaussian was implemented on a steam turbine for stable levitation while the speed ramped through resonant modes [9]. Though stable, the presence of runout or radial oscillation of the turbine was not addressed.

This presents an additional design criterion of reducing and eliminating the sinusoidal disturbance caused by rotor unbalance. A classic method is to utilize the internal model principle and include a model of the disturbance in the feedback path for asymptotic rejection [10]. A sinusoidal internal model was used for sinusoidal tracking of current [11]. However, with a time-varying disturbance, system stability will be difficult to maintain as the internal model is updated. To simultaneously satisfy both stability and rejection criteria, sinusoidal internal models in the form of peak filters were implemented in a parallel loop to reduce vibrations in hard disks [12,13]. In Ref. [14], this was done by designing an internal model through the Youla-parameterization while also updating the controller adaptively. In Ref. [15], a generalized notch filter was cascaded with a prestabilized system to maintain closed-loop stability. However, the coordinate transformation may be cumbersome to include multiple disturbance frequencies.

Repetitive control is another internal model principle-type controller widely used for harmonic rejection. In the prototype repetitive controller (PRC), integer delays are used to generate the internal model at the disturbance's fundamental frequency as well as all its harmonics to the Nyquist frequency [16]. The reduction of the closed-loop sensitivity in so many bands causes amplification in the spectrum at other frequencies; per the Bode sensitivity or so-called "waterbed effect." To provide robustness, a low-pass filter is integrated to reduce the effects of the higher harmonics in the controller [17]. As proven as it is, PRC does exhibit some limitations. First, there is a rather course design tradeoff between stability and performance. The low-pass filter, which protects against modeling uncertainty, also limits the control gains in the pass band. Second, the periodic disturbances PRC is able to affect integer harmonics of the fundamental frequency. For disturbances with nonharmonic makeup, repetitive control is less helpful. Additionally, when using delays, the lengths must be integer valued. In rotor applications, this results in a limited set of speeds disturbance rejection which will be effective. For time-varying disturbance periods, interpolation of delays was proposed in Refs. [18–20].

An internal model principle-based controller using plug-in architecture addresses the AMB–rotor controller design challenges [21,22]. The plug-in structure allows disturbance rejection of specific harmonic frequencies with minimal effect to the stability of the system. The internal model is generated through inversion of cascaded second-order notch filters, providing greater flexibility in tuning performance of the controller while being easily amenable to rotor speed changes. Including notch filters for only those relevant frequencies, coupled with the ability to tune the bandwidth of those notches, greatly reduces the waterbed effect while rejecting multiple frequencies. Furthermore, the frequency location of each notch filter is easily amenable and independent of one another, making this controller attractive to changing rotor speeds as well as more complex harmonic disturbances.

An equally important aspect of this application is to determine the disturbance period accurately. The internal model controller can only be effective if placed at the correct frequency. For systems without reliable sensors, online frequency estimation methods can be applied. Some previous work includes an adaptive algorithm to update an internal model [23]. An adaptive phase-locked loop was used to directly estimate the disturbance

Contributed by the Dynamic Systems Division of ASME for publication in the Journal of Dynamic Systems, Measurement, and Control. Manuscript received October 20, 2014; final manuscript received August 20, 2015; published online October 12, 2015. Assoc. Editor: Ryozo Nagamune.

frequency [24]. A recursive integer period estimation was proposed for adaptive repetitive control [25].

The remainder of this paper is organized as follows: A discussion of the experimental system and its modeling are found in Sec. 2. Section 3 presents the plug-in resonator controller and some of the filter design choices explored. Analysis in performance and stability will be presented. Experimental results and subsequent discussion are presented in Sec. 4. Section 5 summarizes the results of this work.

2 Description of Experimental System

Experimental results were obtained on the MBC500 Turbo, an AMB–rotor system developed by LaunchPoint Technologies. The system consists of a rotor of 303-stainless steel supported at each end by electromagnets. Hall Effect sensors, collocated at each end, measure the gap distance to the rotor and provide positional feedback [26]. The Turbo edition features a shortened shaft specifically designed to push the resonant modes of the system past the maximum rotor speed (Table 1). In Fig. 1, the configuration and coordinate convention of the experimental system are shown. The AMB/sensor pair at each end of the rotor (side-1 or side-2) actuates and senses in the X-plane (horizontal) and the orthogonal Y-plane (vertical). As labeled in the figure, these coordinates are referred to as x_1 and y_1 on one side and x_2 and y_2 on the other. It is apparent that the system is a 4x4 multi-input multi-output (MIMO) system. The axial direction, z, is constrained passively and assumed to have no effect on the dynamics of the system.

2.1 Plant Model. For controller design and analysis, a gray-box model obtained by combining analytical white-box modeling principles with a black-box closed-loop system identification process was used [27].

As discussed in Ref. [27], through the first principles approach, a coordinate transformation is motivated from physical intuition. First, the X-plane and Y-plane motions are assumed to be decoupled. Furthermore, shown in Fig. 2, interplanar coordinates are decoupled from the rotor-end frame into a pure translation and pure rotation of the geometric center of the rotor

$$\begin{pmatrix} x_T \\ x_R \end{pmatrix} = \begin{bmatrix} \frac{1}{2} & \frac{1}{2} \\ \frac{1}{2} & -\frac{1}{2} \end{bmatrix} \cdot \begin{pmatrix} x_1 \\ x_2 \end{pmatrix} \tag{1}$$

To better capture the other non-negligible components (e.g., electromagnets, A/D), a system identification procedure was performed [27]. Because the system is open-loop unstable, a closed-loop identification process was used. A digital signal analyzer performed the sine-sweep to generate the frequency response data from each input to every output. The decoupling procedure is used on the acquired data to produce the four continuous-time single-input single-output systems $[X_T\ X_R\ Y_T\ Y_R]$; corresponding to the *translational* and *rotational* systems of the geometric center of mass in the X- and Y-planes.

Figure 3 shows the decoupled frequency response data (magnitude only for brevity) and their respective low-order fitted models

Table 1 Measurements of rotor shaft for MBC500 turbo

Length	0.147 m
Diameter	0.012 m
First mode	2.4 kHz

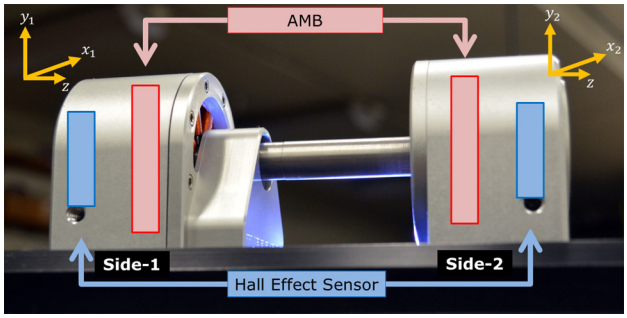

Fig. 1 Actuator–sensor placement of MBC500 turbo

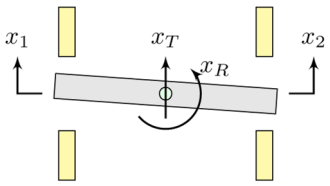

Fig. 2 *X*-plane coordinates (*Y*-plane identical)

$$\begin{aligned} P_{XT} &= \frac{266.9(s^2 + 2126s + 5.47 \times 10^6)}{(s + 2479)(s + 442.8)(s - 460.9)} \\ P_{XR} &= \frac{298.8(s^2 + 942.2s + 2.46 \times 10^6)}{(s + 2240)(s + 394.6)(s - 392.7)} \\ P_{YT} &= \frac{-632.6(s - 1720)(s + 1252)}{(s + 3602)(s + 401.6)(s - 396.2)} \\ P_{YR} &= \frac{-583.6(s - 2639)(s + 1694)}{(s + 4196)(s + 438.3)(s - 447.8)} \end{aligned} \tag{2}$$

The third-order transfer functions of Eq. (2) are more appropriate for control design. The collected data were also used to generate higher-order models, useful for simulation and controller verification.

A couple characteristics of the system drive some design decisions. First, in each of the identified Y-plane systems, there exists one nonminimum phase zero. In subsequent filter development, this detail will prove significant. Another issue to note is the presence of a resonant peak, representing the first bending mode, significant in the two translational axes but not in the two rotational axes due to symmetry. The peak occurs at 2.4 kHz and is not captured by the low-order transfer function. However, it is accounted for and will be motivated by subsequent analysis.

2.2 Stabilizing Controller. AMB systems are open-loop unstable and require a feedback controller for operation. The MBC500 Turbo system is equipped with four analog proportional-derivative controllers. They were, however, replaced with linear-quadratic Gaussian control with integral action (LQGi), C_1, to provide stable and robust levitation of the rotor at the center of the stator over the entire operating speed range.

Though designing feedback control strategies can be effective, one purpose of this work is to demonstrate the benefits and performance achievable implementing a plug-in control module. This is motivated by the fact that in most systems, some feedback controller will already be designed and implemented. An effective complimentary controller can be designed without disturbing the prestabilized system.

2.3 Rotor Speed Measure and Control. The rotor shaft is fitted with turbine blades and a two-way servo valve to spin the rotor. Regulating the speed of the rotor is an important aspect of

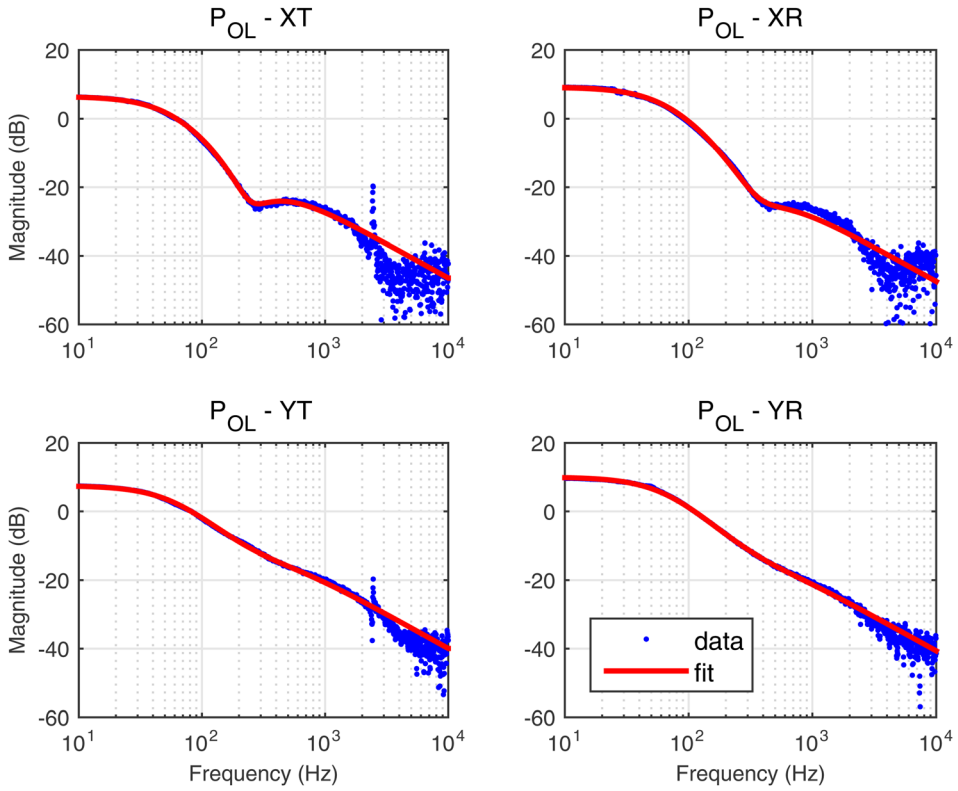

Fig. 3 SysID data versus model fit of decoupled open-loop systems

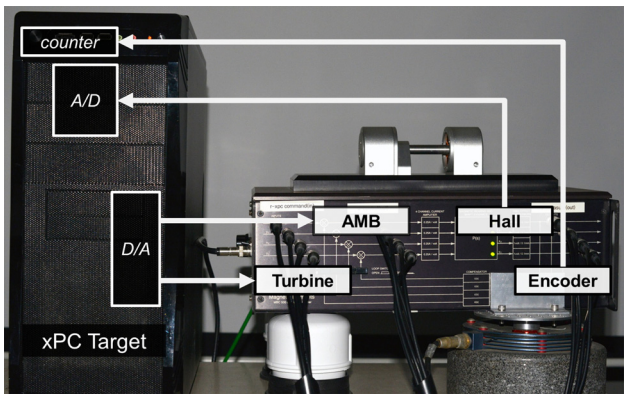

Fig. 4 System hardware

the experiment to the extent that repeatability of the process is required. More importantly, an accurate measure of the rotor speed is required for the controller to perform correctly. The pulses of the onboard encoder are used to trigger a high clock rate (20 MHz) counter card to determine the speed of the rotor. The measured speed is used to close the loop on a proportional-integral-derivative controller for servo valve command.

Stiction was observed to cause hunting of the speed set point, preventing the rotor from reaching any useful constant speed. To counteract stiction in the servo valve, a high-frequency zero-mean dither signal was added to the valve command.

The effectiveness of the proposed control strategy is hinged on the identified disturbance period. The encoder measurement is used to provide an accurate measure.

2.4 Hardware Implementation. Data acquisition and control were implemented using the Mathworks xPC Target platform at a sampling frequency of 10 kHz (Fig. 4). National Instruments

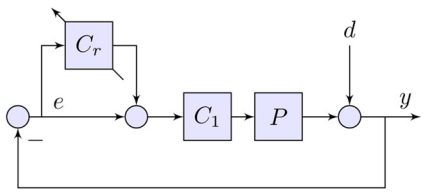

Fig. 5 Addition of plug-in controller *C* to feedback system

PCI-6052e cards were used for data acquisition and command while the PCI-6601 counter card interpreted the encoder.

3 Plug-In Harmonic Resonator

In regulation of the rotor end at the center of the stator, a key disturbance is a result of rotor unbalance. This can be detected as a sinusoidal oscillation of the rotor, otherwise known as runout. A special kind of internal model-based controller for rejecting multiple harmonics was introduced in Ref. [21] and its implementation on the MBC500 was first reported in Ref. [22]. The controller has a unique feature of introducing multiple notches at specified frequencies while minimally perturbing other frequencies on the sensitivity (error rejection). Its design flexibilities make it attractive in addressing the subtleties of rotor operations. The underlying notch filter design provides direct control over the characteristics of the notch. Parameters directly control the depth and bandwidth of the notches which give intuitive handles on the stability and performance of the controller. Furthermore, stability in AMB–rotor application is paramount. To that end, the harmonic resonator is employed as a plug-in unit to a pre-existing feedback loop (Fig. 5). The controller C_1 can be used to provide stability or satisfy other design criteria (e.g., LQGi), while the plug-in controller C_r supplies targeted control effort.

The closed-loop system can be written as $G = (PC_1/(1 + PC_1))$ for simplification. Subsequent design of the plug-in controller is performed on G.

The plug-in controller (C_r) is composed of two filters

$$C_r = D \cdot F \tag{3}$$

the internal model (D) and a stable inversion (F).

3.1 Internal Model Design. The internal model principle requires a model of the disturbance to be placed in the feedback path [10]. Ideally, a filter L is designed to satisfy the criteria

$$L = \begin{cases} L(e^{j\omega}) = 1 \text{ if } \omega = \omega_{k=1,2,\ldots p} \\ L(e^{j\omega}) \approx 0 \text{ if } \omega \neq \omega_k \end{cases} \tag{4}$$

where the filter reaches unity at a p-number of frequencies. Then, by placing L in a positive-feedback loop, the output of the loop will produce infinite control gain at the specified frequencies and zero elsewhere.

In this paper, filter L is realized by first designing a p-number of cascaded second-order notch filters defined by

$$H(z^{-1}) = \prod_{k=1}^{p} \frac{1 - 2\beta_k \cos\omega_k z^{-1} + \beta_k^2 z^{-2}}{1 - 2\rho_k \cos\omega_k z^{-1} + \rho_k^2 z^{-2}} \tag{5}$$

This formulation makes specifying key parameters of the internal model straightforward. The parameter ω_k in Eq. (5) represents the location of the notch in the Nyquist band and it is quite apparent that any frequency can be specified, including noninteger speeds. In comparison, repetitive control has a limited set of allowable rotor disturbance periods since the delay lengths are required to be integer valued. Even with fractional delay solutions, these are approximations which reduce performance.

Though repetitive controllers generate control at all the overtones of the disturbance period, in general, the Fourier components of the disturbance signal may not necessarily share any relative relationship among them (e.g., integer harmonics). There may also only exist a small number of relevant components in the signal. In these cases, repetitive control could be both over- and underdesigned for the disturbance at hand. By cascading notch filters, Eq. (5) can provide compensation at the appropriate frequencies with the freedom of independently selecting these frequencies.

Furthermore, by using this second-order notch filter as the basis, we can take advantage of the direct control over the characteristic of each notch. Parameters of the filter, ρ and β, shape the depth and bandwidth. They can be tuned independently for each kth frequency. The two factors are chosen to satisfy the relationship $0 \ll \rho < \beta \leq 1$. For the notch filter, $\beta = 1$ places the zeros on the unit circle producing zero filter output. Once it is inverted, the peak is at unity and will produce infinite gain in the feedback loop. The parameter ρ controls radius of the poles of H. As $\rho \to 1$, the filter becomes more ideal in that frequencies away from the notch are less affected while $\rho < 1$ is maintained to keep the poles inside the unit circle to produce a stable filter.

The relationship between the two factors can be used to approximate the -3 dB bandwidth through the expression

$$BW_{\text{Hz}} \approx \frac{\pi(\beta_k - \rho_k)}{2\pi T_s} \tag{6}$$

where T_s is the sample time of the discrete time system. A wider notch provides faster convergence as well as robustness to mismatches between the disturbance and controller frequencies. This must be balanced by the so-called waterbed effect, which describes the resulting amplification in another part of the spectrum resulting in a loss of performance and stability.

The peak filter is made by inverting the notch filter

$$L(z^{-1}) = 1 - H(z^{-1}) \tag{7}$$

Additionally, constructing the peak filter through this notch-filter-inversion process allows the "tails" of the peaks to fall to zero, instead of unity, further satisfying Eq. (4).

In Fig. 6, the internal model is generated by wrapping the peak filter in a positive-feedback loop

$$D(z^{-1}) = \frac{L(z^{-1})}{1 - L(z^{-1})} \tag{8}$$

3.2 Stability Condition and Inversion Filter F. Filter F is included to satisfy a stability condition derived from the Nyquist stability criterion. A detailed discussion can be found in Ref. [21]. The stability condition can be derived from Fig. 5

$$||L(1 - FG)||_\infty < 1 \tag{9}$$

where G is the prestabilized system. This is easily satisfied in the majority of the spectrum by the design of L from Eq. (4). Where $L = 1$ by design, the condition is met by choosing the filter which satisfies $F(e^{j\omega}) \approx G^{-1}(e^{j\omega})$.

3.2.1 Zero-Phase Error Inversion Filter. Taking into account, the nonminimum phase systems of the Y-plane, one possible method of satisfying Eq. (9) is the zero-phase error controller (ZPEC) [28]. It is a useful approximate inversion method for plants with nonminimum phase zeros since a direct inversion would produce an unstable filter. For a factorization of the stable system

$$G(z^{-1}) = \frac{z^{-d} B^+(z^{-1}) B^-(z^{-1})}{A(z^{-1})} \tag{10}$$

d represents the relative system order, and A, B^+, and B^- are the poles, stable zeros, and unstable zeros, respectively. The ZPEC inversion is defined as

$$F_{\text{ZPEC}}(z^{-1}) = \frac{A(z^{-1})[B^-(z^{-1})]^*}{\gamma z^{-d} B^+(z^{-1})} \tag{11}$$

where $[B^-(z^{-1})]^*$ is the complex conjugate of the unstable zeros. This produces the cascaded system $F_{\text{ZPEC}}G = [(B^-(z^{-1})[B^-(z^{-1})]^*)/\gamma]$, which has zero phase since the zeros are complex conjugates of one another.

Depending on the locations of the unstable zeros, the corresponding magnitude response may be unfavorable. Nonminimum phase zeros near the unit circle result in a filter which generates high gains near the Nyquist frequency [29]. To maintain stability, the constant $\gamma = [B^-(e^{j\omega})][B^-(e^{-j\omega})]$ is used to scale the magnitude of the filter output to unity at the prescribed frequency (Fig. 7, dashed-dot).

Despite the idealized design of L in Eq. (4), the high pass magnitude response of ZPEC was found to excite the resonant modes of the translational systems found in Fig. 3. A notch was designed to filter out the control component at 2.4 kHz. As the feedback controller itself did not excite this mode, and to emphasize the utility of the plug-in approach on an inherited closed-loop system, the notch was placed in series with ZPEC in the plug-in controller (Fig. 7). Subsequent analysis and experiments will reference this filter design.

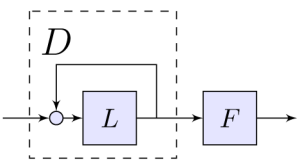

Fig. 6 Components of harmonic resonator (C_r)

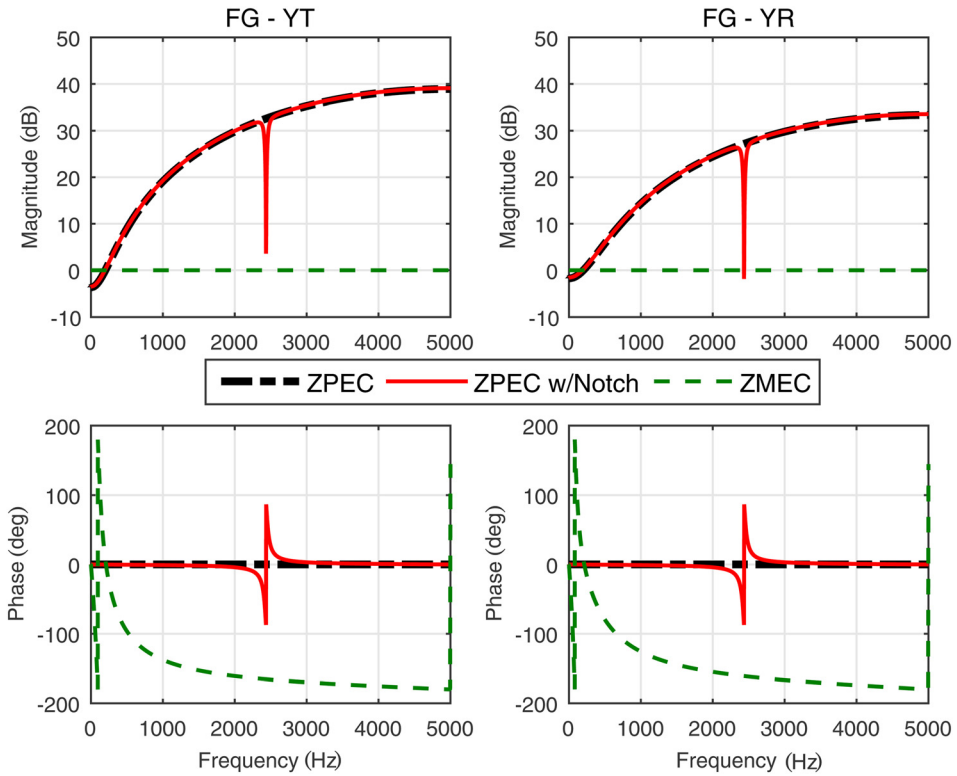

Fig. 7 *FG* comparison for various *F* designs at 200 Hz

3.2.2 Zero Magnitude Error Inversion Filter. To counteract the magnitude amplification at high frequencies, another model inversion filter with more favorable magnitude characteristics is considered. The zero magnitude error control (ZMEC) is a similar approximate model inversion technique, when faced with nonminimum phase zeros, will invert the magnitude rather than the phase [30]. The filter is defined as

$$F_{\text{ZMEC}}(z^{-1}) = \frac{A(z^{-1})}{z^{-d}B^{+}(z^{-1})[B^{-}(z^{-1})]^{*}} \tag{12}$$

and produces $F_{\text{ZMEC}}G = [B^{-}(z^{-1})/([B^{-}(z^{-1})]^{*})]$ which is essentially an all-pass filter with unit magnitude. The magnitude response is thus more favorable as compared to ZPEC. The phase, however, must be compensated similar to the role of γ in ZPEC. Generally, an additional all-pass filter F_{ap}

$$F_{\text{ap}}(z^{-1}) = \frac{r^2 - 2\cos(\omega_{\text{ap}})z^{-1} + z^{-2}}{1 - 2\cos(\omega_{\text{ap}})z^{-1} + r^2 z^{-2}} \tag{13}$$

is designed and cascaded to adjust the phase. The corner frequency ω_{ap} determines where the phase is $-\pi$ and the parameter r affects the sharpness of the transition. By first determining the phase of $F_{\text{ZMEC}}G(e^{j\omega})$, the necessary phase compensation can be determined and an appropriate ω_{ap} can be calculated to provide compensation (Fig. 7, dashed).

3.2.3 Causal Implementation. For strictly proper systems and/or those with nonminimum phase zeros, the resulting inversions will be noncausal. They must be provided with enough "look-ahead" or "preview" steps to form a causal filter. Separating into a causal filter and noncausal previews

$$z^{m_1}F_{\text{ZPEC,caus}} = z^{m_1}\frac{A(z^{-1})[B^{-}(z^{-1})]^{*}}{\gamma z^{(d+2n_u)}B^{+}(z^{-1})} \tag{14}$$

$$z^{m_2}F_{\text{ZMEC,caus}} = z^{m_2}\frac{A(z^{-1})}{z^{d}B^{+}(z^{-1})[B^{-}(z^{-1})]^{*}} \cdot F_{\text{ap}} \tag{15}$$

where n_u is the number of unstable zeros and $m_1 = d + n_u$ and $m_2 = d$ represent the preview requirement for each respective filter.

A property of the peak filter formulation can be exploited in that L is a relative order of one. This allows the internal model to absorb a preview step. To compensate n-step previews, the notch filter can be up-sampled to

$$H_n(z^{-1}) = \prod_{k=1}^{p}\frac{1 - 2\beta_k\cos n\omega_k z^{-n} + \beta_k^2 z^{-2n}}{1 - 2\rho_k\cos n\omega_k z^{-n} + \rho_k^2 z^{-2n}} \tag{16}$$

Then, Eq. (7) would produce a peak filter with n-relative order. Thus, an n-step preview requirement can be compensated by the up-sampled filter and $L_n z^n$ will remain proper. However, directly applying Eq. (7) to produce L_m will cause $(m-1)$ aliased peaks to show up in the band at locations

$$\omega_{k,i} = \left|\left(\omega_k \pm \frac{2\pi i}{m}\right)\text{mod}(2\pi)\right| \tag{17}$$

where $i \in \mathbb{Z}$ between $0 \le i \le \lfloor m/2 \rfloor$. The aliased peaks are removed while maintaining the correct filter order by combining two filters such that for an m-step preview requirement

$$L_m(z^{-1}) = L_1 L_{(m-1)} \tag{18}$$

For a given system, F_{ZMEC} will require less lifting of L (i.e., only for relative order) and yield comparatively wider notches.

3.3 Sensitivity and Stability Analysis. Analysis of the sensitivity function can be insightful as a measure of performance. The block diagram of Fig. 5 can be simplified to produce

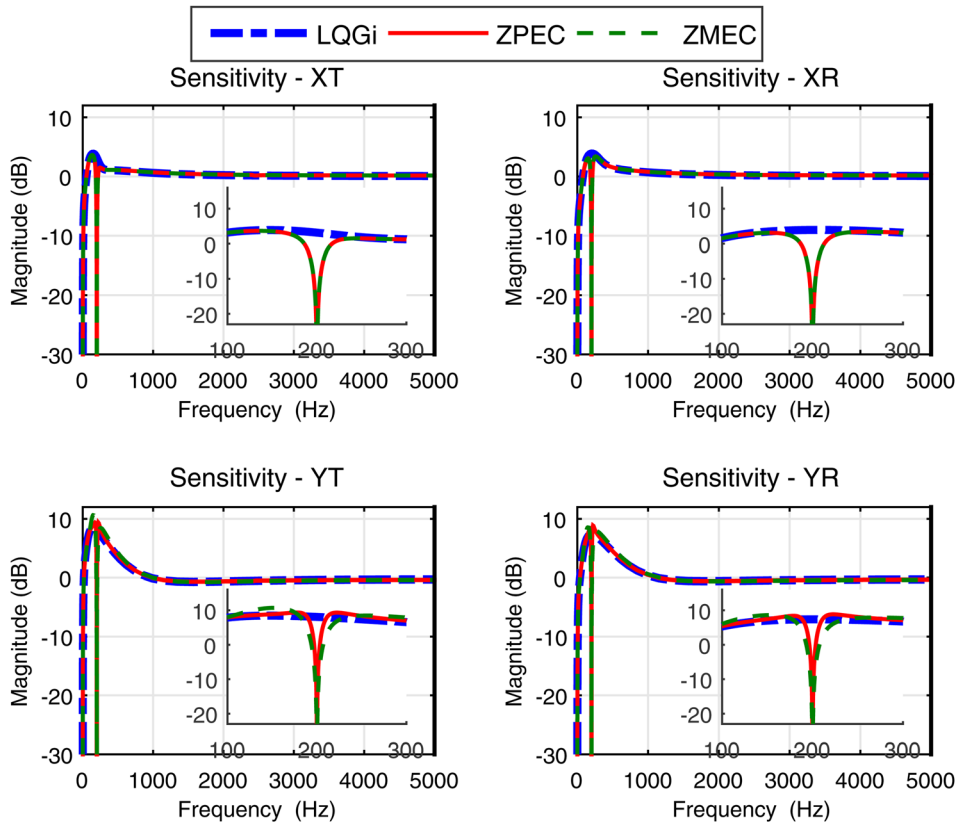

Fig. 8 Sensitivity function of plug-in resonators

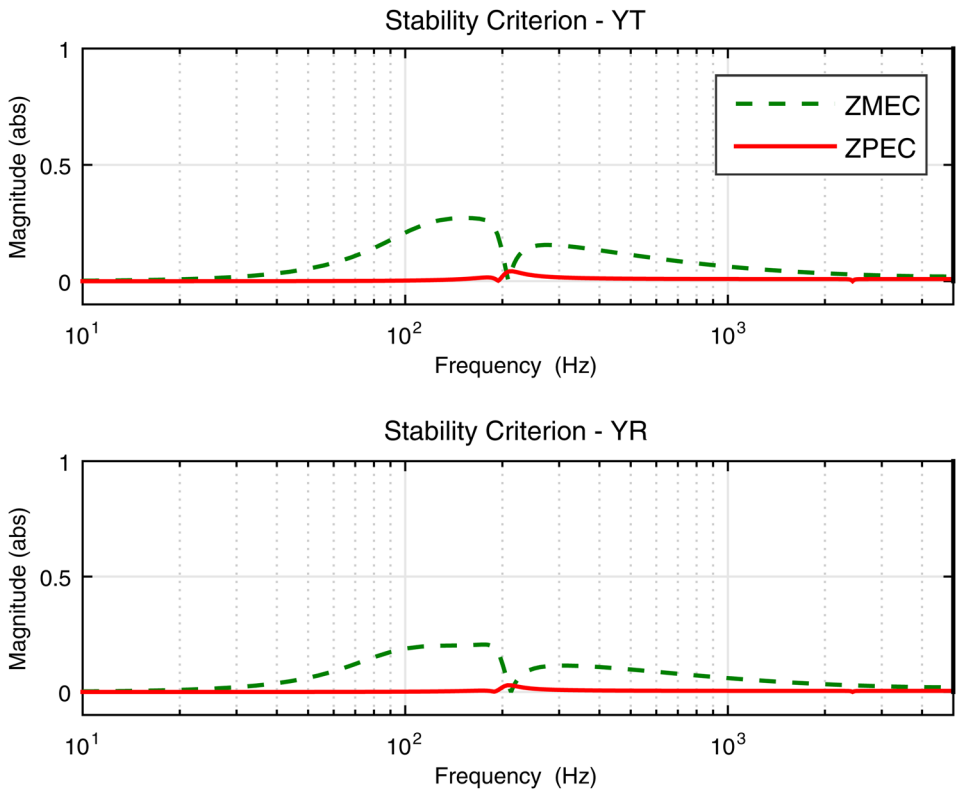

Fig. 9 Stability criterion (Eq. (9)) of *Y*-plane systems

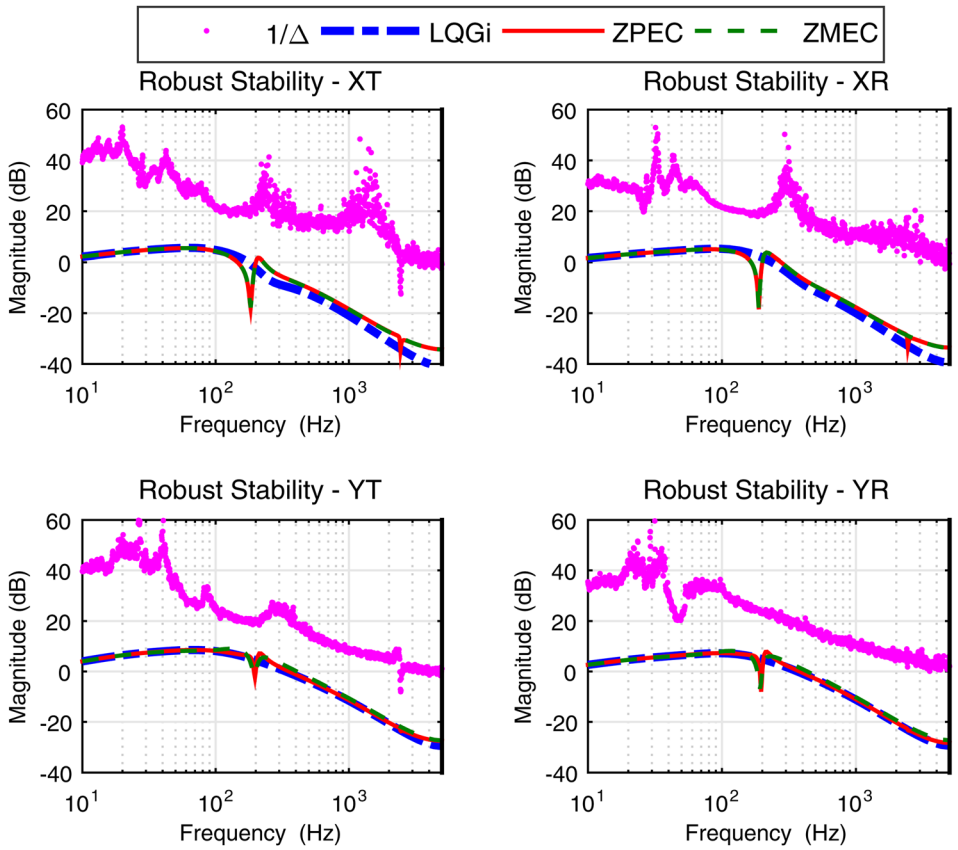

Fig. 10 Robust stability of plug-in resonator

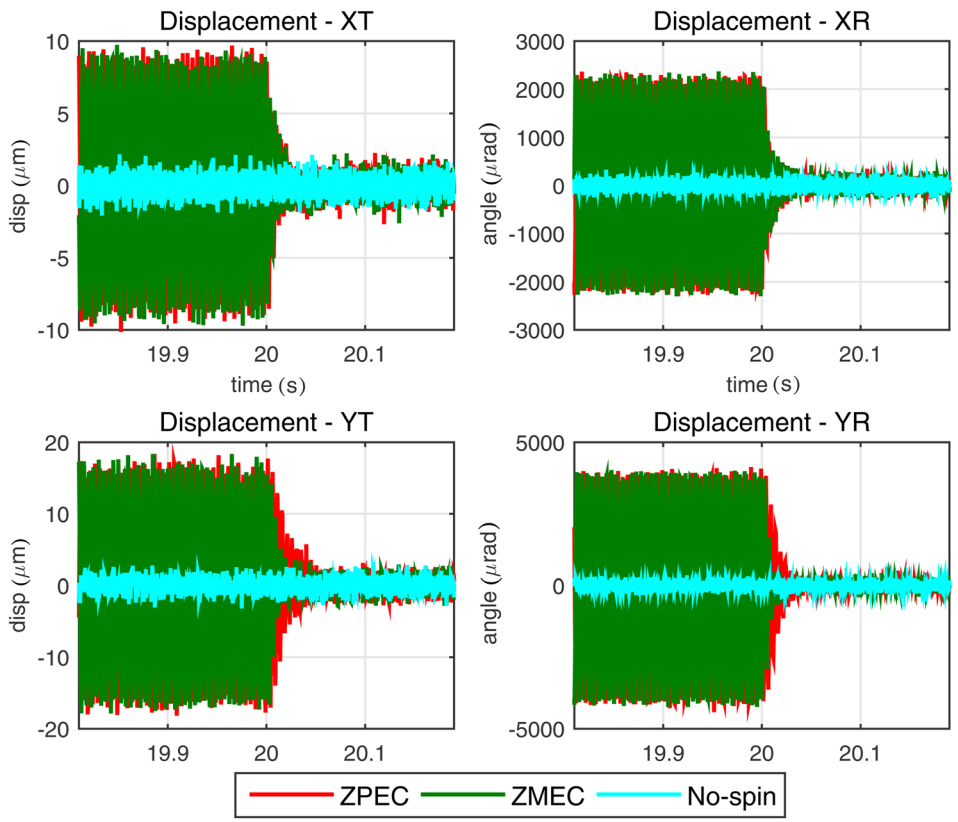

Fig. 11 Rotor displacement—plug-in resonator using ZPEC and ZMEC inversion

$$S = S_{C1} \cdot S_{C_r} = \frac{1}{1 + PC_1} \cdot \frac{1}{1 + GC_r} \tag{19}$$

where G is the closed-loop transfer function. This factorization highlights the property of the plug-in structure where the sensitivity of the underlying prestabilized loop (S_{C1}) is narrowly altered by the addition of the new controller. Plug-in controller C_r is designed using the closed-loop plant G.

Figure 8 compares the sensitivity functions for plug-in controllers designed using the inversion methods described. The sensitivity of the prestabilized plant S_{C_1} is included in blue. It may be noted that in much of the spectrum, the transfer functions overlap greatly. As expected from Eq. (19), the sensitivity function of the closed-loop system is modified only at the designed frequencies. The insets plot in each respective subplot highlights the effect of the peak resonator in reducing the sensitivity to disturbances in that band.

To ensure a fair comparison, the parameters of peak and inversion were chosen identically where appropriate. This is verified by the identical controllers for the X-plane systems. Since these systems are minimum phase systems, both inversions yield the same filter.

The differences in the Y-plane systems are a result of how each algorithm handles the unstable zero. Because the ZPEC method will always require more lifting, the resulting peak filter construction in Eq. (18) effectively narrows the bandwidth for the same notch parameters. For a notch filter, the convergence can be determined by the parameter ρ, where a smaller ρ yields faster convergence [20]. In other words, a wider notch bandwidth converges faster, as well as being more robust to a mismatch in the identified disturbance frequency. Consequently, a wider notch means more pronounced ripples in the spectrum. This is evident in the inset plots of the Y-plane system in Fig. 8. The notch formed by ZMEC (green) is wider than ZPEC (red), while suffering from larger amplification (ripple) in the regions near the notch.

It should be noted that it is also more challenging to design a satisfactory ZMEC filter. Since the all-pass filter for frequency compensation must be designed to correct the phase at each targeted frequency, multiple all-pass sections may be required. The addition of each filter will affect the phase of the previously compensated regions. This leaves an iterative design process for multiple targeted frequencies. This also makes the time-varying rotor condition challenging to implement.

Stability is especially critical to rotor operations as it directly equates to safety. As one measure of stability, the criterion in Eq. (9) is verified. Nominally, a complete inversion of the X-plane plants can be found resulting in the left-hand side of Eq. (9) evaluating to 0. Thus, only the nontrivial results for the Y-plane systems are shown in Fig. 9.

Though the unstable zeros result in high magnitudes for the ZPEC formulation, by using γ to scale crossing, the L filter works in tandem to satisfy the criteria. Likewise, the ZMEC formulation satisfies the stability criterion. In the transition between the two filters, the magnitude increase is caused by the imperfect phase compensation in the transition band of the all-pass filter.

Table 2 Root-Mean-Square (RMS) of steady-state displacement—plug-in resonator using ZPEC and ZMEC inversion

	LQGi (200 Hz)	ZPEC (200 Hz)	ZMEC (200 Hz)	Levitate only	Sensor noise
XT (μm)	5.71	0.66	0.65	0.59	0.57
XR (μrad)	1509.6	95.09	95.21	88.25	85.55
YT (μm)	11.20	0.98	1.01	0.84	0.75
YR (μrad)	2770.3	121.31	124.44	111.76	103.01

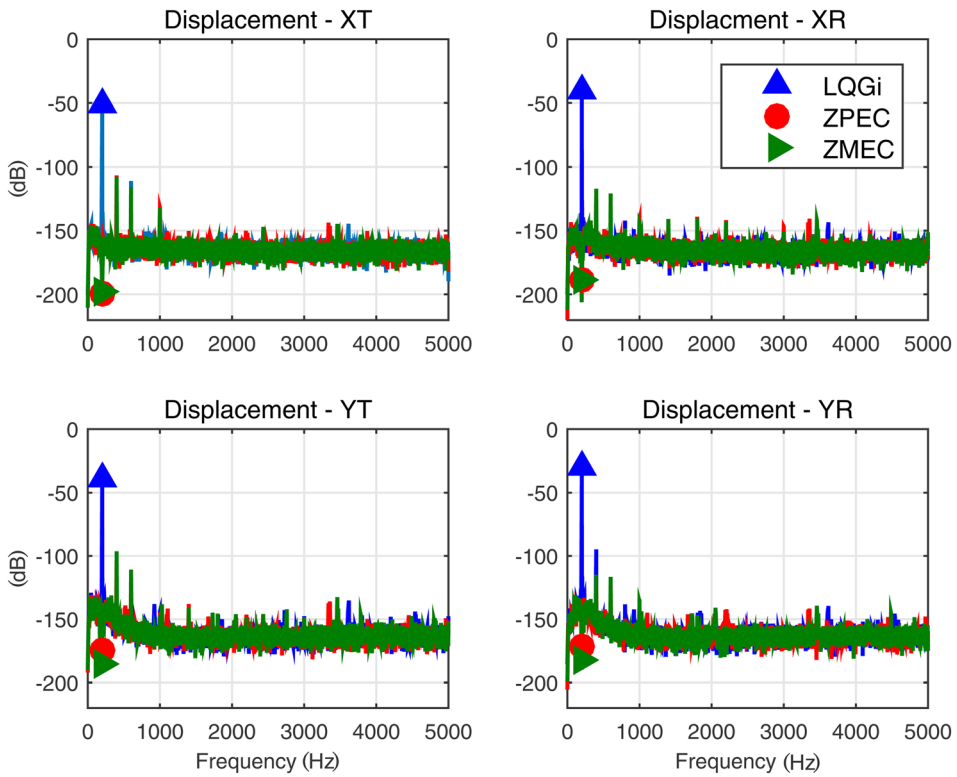

Fig. 12 Rotor displacement spectrum—plug-in resonator using ZPEC and ZMEC

The robustness of the system is also a useful analysis to perform. The robust stability criterion can be defined as

$$T = \frac{C_1 P(1+DF)}{1+C_1 P(1+DF)} \tag{20}$$

$$\left| \frac{C_1 P(1+DF)}{1+C_1 P(1+DF)} \right| \leq \frac{1}{|\Delta|} \tag{21}$$

where the multiplicative modeling error, Δ, of the open-loop systems was produced in Ref. [27]. The results of Fig. 10 validate the designs. The robustness of the feedback controller is mainly preserved with the addition of the plug-in resonator.

For the ZPEC controller, the dip at 2.4 kHz indicates the designed notch filter ensuring that the resonant mode is not excited.

4 Experimental Results

In the experiments presented, the plug-in resonator is used to reject sinusoidal disturbances on the MBC500 Turbo. Steady-state and time-varying rotor speed conditions are examined as well as controller design configurations. The internal model is updated using the encoder measurements at the control loop rate of 10 kHz.

4.1 Transient Performance of Resonator. The plug-in resonators designed in Sec. 3 were applied to the MBC500 Turbo for a constant speed condition. In the time trace of Fig. 11, the rotor is spun to the desired speed (200 Hz) under feedback control only. The peak resonator is connected at $t = 20s$ and the resulting transient performance can be observed. Disturbance rejection occurs

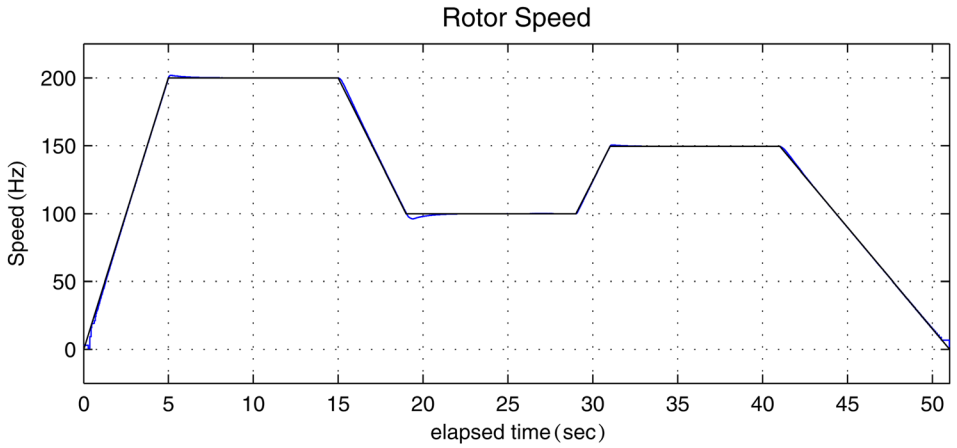

Fig. 13 General rotor speed profile

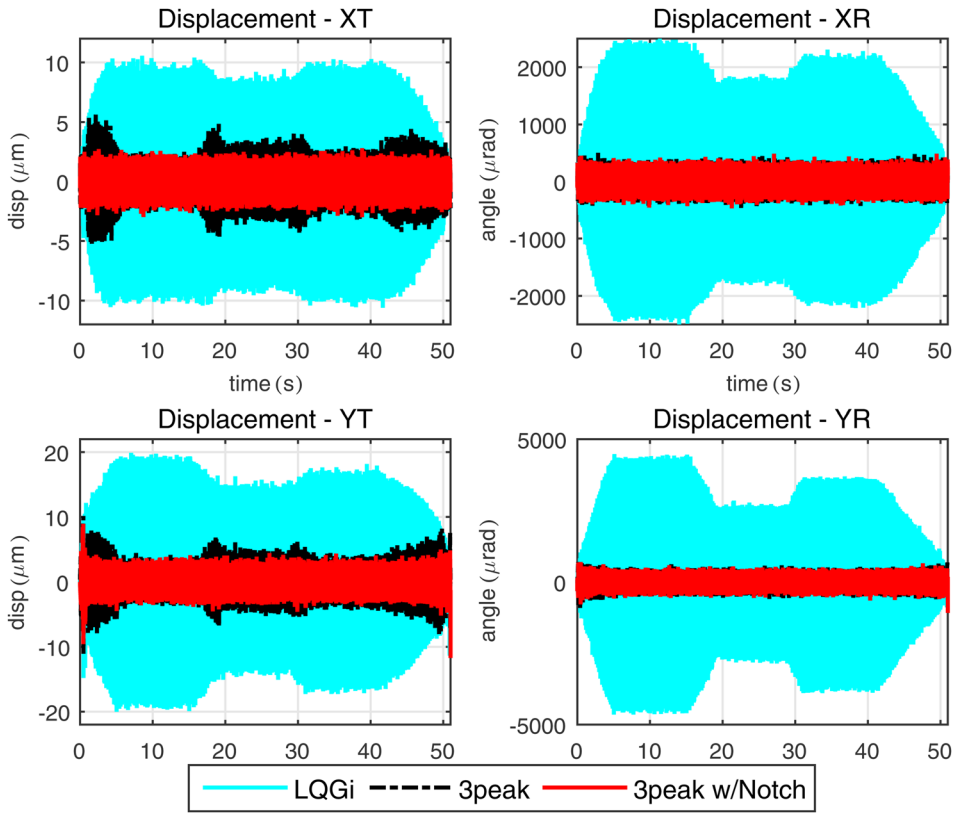

Fig. 14 Rotor displacement—three-peak plug-in resonator for varying speeds

quickly as the displacements of the four systems reach their steady-state value in less than 0.1 s in all four axes.

Both ZPEC and ZMEC inversion methods are implemented and compared. The X-plane systems produce identical traces since these methods yield the same inversion filter. The narrower sensitivity notches of ZPEC (Fig. 8) reduce the convergence rate compared to ZMEC.

The RMS of the displacement is organized in Table 2. The displacements are shown in the decoupled transformed coordinates. The translational systems are measured in microns, while the rotational systems are in microradians. Column "LQGi" represents the stable levitation of the rotor during constant rotational velocity. The RMS is clearly larger due to the strong disturbance caused by rotor unbalance. Implementing the plug-in resonator with both ZPEC and ZMEC inversion techniques shows large reductions indicating the rotor is spinning tighter about its geometric axis and appropriate rejection is taking place. Since $\beta = 1$ in both peak filter designs, the steady-state performance is identical.

Two additional rotor conditions are included. With the LQGi loop closed, the rotor is regulated at the center of the stator. Without any angular velocity, "levitate only" represents a best-case in terms of disturbance rejection. For completeness, the "sensor noise" is also provided to quantify the noise floor of the system. No control action is applied and the rotor is resting against the stator. After removing the bias from this signal, the resulting RMS provides a baseline reading.

Table 3 RMS of decoupled output—three-peak plug-in for varying speeds

	LQGi	Three-peak	Three-peak w/notch	Levitate only
XT (μm)	5.23	1.17	0.60	0.59
XR (μrad)	1231.6	97.27	95.05	88.25
YT (μm)	9.60	1.60	0.97	0.84
YR (μrad)	2182.4	135.57	129.75	111.76

Both plug-in resonator designs, containing one-peak in the internal model, nearly achieve the ideal rejection mark. The radial vibration in rotor unbalance primarily consists of the primary harmonic at the rotor speed. Thus, designing the filter to target this frequency yields the most significant rejection performance. Though additional performance can be gained by designing more peaks in the internal model, the diminishing returns on effort can also be considered.

The spectral components of the displacement can be examined for additional insight into control performance. From Fig. 12, when only LQGi is used to stabilize the rotor, the largest spectral component is clearly the shaft speed of 200 Hz, though harmonics of the disturbance are also clearly present. In comparison, the plug-in controllers achieve complete rejection of the designed frequency. The peaks at the second and third harmonics of the rotor speed are unaltered, along with the rest of the spectrum which remains unchanged.

4.2 Disturbance Rejection for Varying Rotational Speeds. In this experiment, the plug-in resonator for disturbance rejection under time-varying rotor speeds is examined. The velocity profile in Fig. 13 was applied, though achieving this trajectory is less important than measuring the actual instantaneous velocity of the rotor and placing the peaks at the correct frequencies. The encoder measurement updates the peak filter frequency, at the control loop rate, to place the internal model at the correct position.

From examining the initial power spectral density (PSD) in Fig. 12, the second and third harmonics of the rotor speed also contribute to the disturbance and are natural extensions of the controller. The ZPEC inversion is used to ensure phase compensation over the rotor speed range. The gain γ can be scheduled easily according to the measured rotor speed and provides some stability against the high magnitude of ZPEC. Though ZMEC would produce an ideal magnitude response, the phase compensation aspect made implementation for multiple peaks/time-varying rotor speed difficult.

In these subsequent results, the plug-in resonator is designed to compensate the three harmonic disturbances (three-peak) and uses the ZPEC inversion.

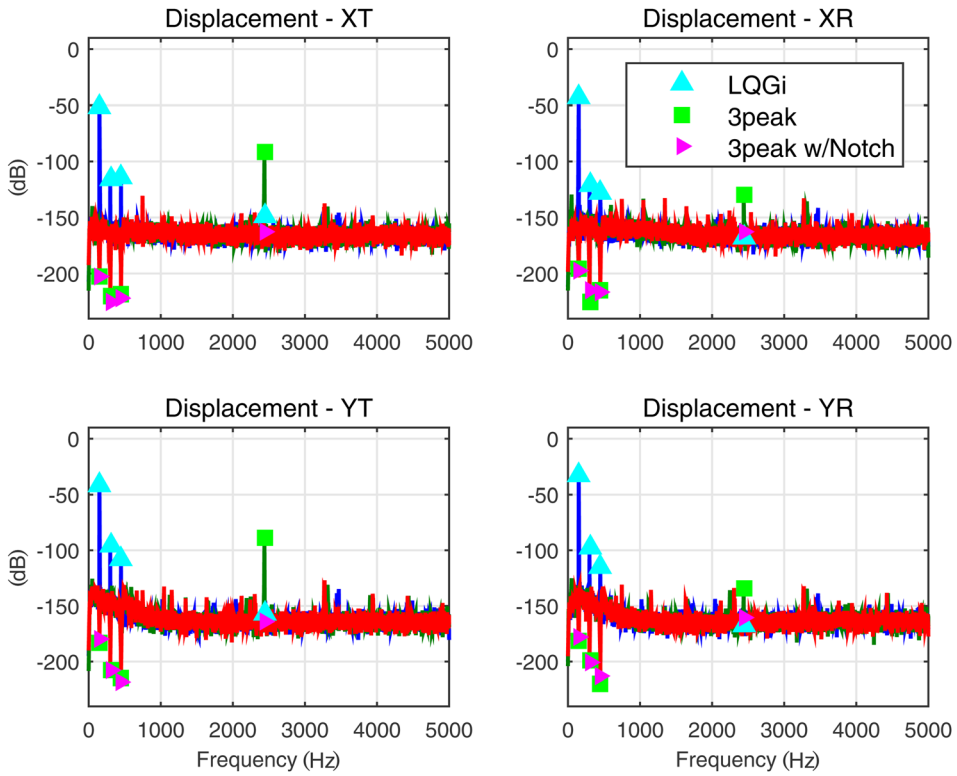

Fig. 15 Rotor displacement spectrum—three-peak plug-in resonator at $36 \le t \le 41$ s

This profile represents a general velocity change in rotor systems between various set points. The profile was selected to emphasize the various capabilities of the plug-in harmonic resonator. The velocity set points are specified to 200 Hz, 100 Hz, and 149.4 Hz to demonstrate the flexibility of disturbance rejection. The rates of acceleration and deceleration are also selected with similar intent.

The plug-in resonator is connected throughout the entire run to reduce runout at all rotor speeds. Figure 14 compares the measured displacements with and without the plug-in controller. Additionally, the inversion methods for ZPEC with and without the notch filter (Fig. 7) are implemented. The plug-in controller reduces the large amplitude displacements, though there is performance degradation in the translational systems when using the three-peak resonator. This is explained by the resonant mode excitation alluded to from Fig. 3. When utilizing the control notch approach (w/Notch), more consistent disturbance rejection performance throughout the run is observed. The RMS of the displacements is compared in Table 3 over the entire run.

Figure 15 shows the PSD during $36\,\text{s} \leq t \leq 41\,\text{s}$ corresponding to a rotor speed of 149.4 Hz. This section was chosen to demonstrate performance when the disturbance period is not integer valued nor a multiple of the sample period. Note the excitation of the 2.4 kHz mode in the translational systems when using the standard three-peak-ZPEC controller. The fact that LQGi does not excite this mode indicates that this stems from the plug-in controller. The three-peak-w/Notch controller addresses this issue and the bending mode remains unexcited.

5 Conclusion

In this paper, a plug-in resonator based on the internal model principle was applied to reject harmonic disturbances in an AMB–rotor system. The internal model is realized through cascaded notch filters, which allows for the rejection of multiple, easily updated frequencies, making this controller attractive and effective for time-varying disturbance periods. The plug-in structure minimally disturbs the stability of the prestabilized closed-loop system. Results presented show effective disturbance rejection performance that regulates outputs to near sensor-noise levels.

References

[1] Schweitzer, G., Bleuler, H., and Traxler, A., 1994, *Active Magnetic Bearings—Basics, Properties and Applications of Active Magnetic Bearings*, Vdf Hochschulverlag, Zurich, Switzerland.

[2] Barney, P., Laugger, J., Petteys, R., Redmond, J., and Sullivan, W., 1999, "Adaptive Spindle Balancing Using Magnetically Levitated Bearings," International Mechanical Engineering Congress and Expo.

[3] Shi, J., and Lee, W. S., 2009, "Analytical Feedback Design Via Interpolation Approach for the Strong Stabilization of a Magnetic Bearing System," Control and Decision Conference, Guilin, June 17–19, pp. 274–279.

[4] Chen, X., Ji, L., and Liu, K., 2010, "A BP Neural Network Controller for Magnetic Suspended Flywheel System," 3rd IEEE International Conference on Computer Science and Information Technology (ICCSIT), Vol. 6, pp. 448–452.

[5] Zhang, X., Shinshi, T., Li, L., Choi, K. B., and Shimokohbe, A., 2001, "Precision Control of Radial Magnetic Bearing," 10th International Conference on Precision Engineering, Yokohama, Japan, July 18–20, pp. 714–718.

[6] Hoshi, H., Shinshi, T., and Takatani, S., 2006, "Third-Generation Blood Pumps With Mechanical Noncontact Magnetic Bearings," Artif. Organs, **30**(5), pp. 324–338.

[7] Knospe, C. R., Hope, R. W., Fedigan, S. J., and Williams, R. D., 1995, "Experiments in the Control of Unbalance Response Using Magnetic Bearings," Mechatronics, **5**(4), pp. 385–400.

[8] Seto, H., Namerikawa, T., and Fujita, M., 2006, "Experimental Evaluation on h_∞ DIA Control of Magnetic Bearings With Rotor Unbalance," 10th International Symposium on Magnetic Bearings, Hotel du Parc, Martigny, Switzerland, pp. 82–87.

[9] Yang, G., Xu, Y., Shi, Z., and Gu, H., 2007, "Characteristic Analysis of Rotor Dynamics and Experiments of Active Magnetic Bearing for HTR-10GT," Nucl. Eng. Des., **237**(12–13), pp. 1363–1371.

[10] Francis, B., and Wonham, W., 1976, "The Internal Model Principle of Control Theory," Automatica, **12**(5), pp. 457–465.

[11] Fukuda, S., and Imamura, R., 2005, "Application of a Sinusoidal Internal Model to Current Control of Three-Phase Utility-Interface Converters," IEEE Trans. Ind. Electron., **52**(2), pp. 420–426.

[12] Kim, Y. H., Kang, C. I., and Tomizuka, M., 2005, "Adaptive and Optimal Rejection of Non-Repeatable Disturbance in Hard Disk Drives," IEEE/ASME International Conference on Advanced Intelligent Mechatronics, pp. 1–6.

[13] Zheng, Q., and Tomizuka, M., 2007, "Compensation of Dominant Frequency Components of Nonrepeatable Disturbance in Hard Disk Drives," IEEE Trans. Magn., **43**(9), pp. 3756–3762.

[14] Landau, I. D., Constantinescu, A., and Rey, D., 2005, "Adaptive Narrow Band Disturbance Rejection Applied to an Active Suspension—An Internal Model Principle Approach," Automatica, **41**(4), pp. 563–574.

[15] Herzog, R., Bühler, P., Gähler, C., and Larsonneur, R., 1996, "Unbalance Compensation Using Generalized Notch Filters in the Multivariable Feedback of Magnetic Bearings," IEEE Trans. Control Syst. Technol., **4**(5), pp. 580–586.

[16] Tomizuka, M., Tsao, T. C., and Chew, K. K., 1989, "Analysis and Synthesis of Discrete-Time Repetitive Controllers," ASME J. Dyn. Syst. Meas. Control, **111**(3), pp. 353–358.

[17] Tsao, T. C., and Tomizuka, M., 1994, "Robust Adaptive and Repetitive Digital Tracking Control and Application to a Hydraulic Servo for Noncircular Machining," ASME J. Dyn. Syst. Meas. Control, **116**(1), pp. 24–32.

[18] Yu, S. H., and Hu, J. S., 2000, "Asymptotic Rejection of Periodic Disturbances With Fixed or Varying Period," ASME J. Dyn. Syst. Meas. Control, **123**(3), pp. 324–329.

[19] Tammi, K., Hätönen, J., and Daley, S., 2007, "Novel Adaptive Repetitive Algorithm for Active Vibration Control of a Variable-Speed Rotor," J. Mech. Sci. Technol., **21**(6), pp. 855–859.

[20] Wang, Y., Wang, D., Zhang, B., and Zhou, K., 2007, "Fractional Delay Based Repetitive Control With Application to PWM DC/AC Converters," IEEE International Conference on Control Applications, Singapore, Oct. 1–3, pp. 928–933.

[21] Wang, Y., Chu, K., and Tsao, T. C., 2009, "An Analysis and Synthesis of Internal Model Principle Type Controllers," American Control Conference, St. Louis, MO, June 10–12, pp. 488–493.

[22] Kang, C., and Tsao, T. C., 2014, "Control of Magnetic Bearings With Plug-In Time-Varying Harmonic Resonators," American Control Conference, Portland, OR, June 4–6, pp. 4237–4242.

[23] Brown, L. J., and Zhang, Q., 2004, "Periodic Disturbance Cancellation With Uncertain Frequency," Automatica, **40**(4), pp. 631–637.

[24] Bodson, M., and Douglas, S. C., 1997, "Adaptive Algorithms for the Rejection of Sinusoidal Disturbance With Unknown Frequency," Automatica, **33**(12), pp. 2213–2221.

[25] Tsao, T. C., Qian, Y.-X., and Nemani, M., 2000, "Repetitive Control for Asymptotic Tracking of Periodic Signals With an Unknown Period," ASME J. Dyn. Syst. Meas. Control, **122**(2), pp. 364–369.

[26] Paden, B., Morse, N., and Smith, R., 1996, "Magnetic Bearing Experiment for Integrated Teaching and Research Laboratories," IEEE International Conference on Control Applications, Dearborn, MI, Sept. 15–18, pp. 421–425.

[27] Chu, K., Wang, Y., Wilson, J., Lin, C. Y., and Tsao, T. C., 2010, "Modeling and Control of a Magnetic Bearing System," American Control Conference, Baltimore, MD, June 30–July 2, pp. 2206–2211.

[28] Tomizuka, M., 1987, "Zero Phase Error Tracking Algorithm for Digital Control," ASME J. Dyn. Syst. Meas. Control, **109**(1), pp. 65–68.

[29] Butterworth, J. A., Pao, L. Y., and Abramovitch, D. Y., 2012, "Analysis and Comparison of Three Discrete-Time Feedforward Model-Inverse Control Techniques for Nonminimum-Phase Systems," Mechatronics, **22**(5), pp. 577–587.

[30] Rigney, B. P., Pao, L. Y., and Lawrence, D. A., 2009, "Nonminimum Phase Dynamic Inversion for Settle Time Applications," IEEE Trans. Control Syst. Technol., **17**(5), pp. 989–1005.